Chapter 4

Stimuli Responsive Structural Transitions in Aqueous 16-Isb-16

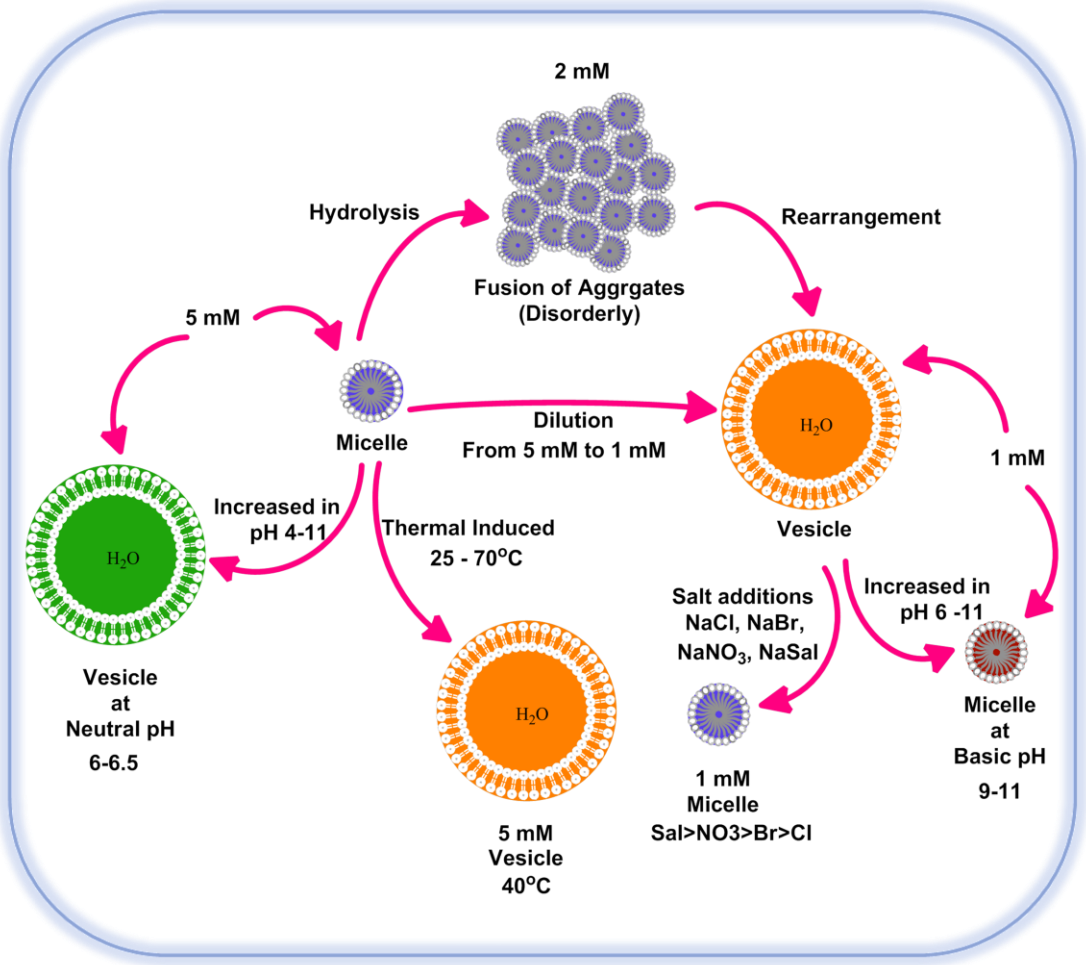

4.1. Introduction

Among surfactant morphologies (spherical micelle, elpsoidal micelle, rod shape micelle, worm like micelle, vesicle, helical structure or tubelar shape) that have been obtained so far, vesicle has attracted much attention becuase they can serve different purposes such as biological model membrane [1,2], containers for encapsulation and evantual release of drugs [3] and microreactor for the formation of a range of inorganic nanoparticles [4]. In particular, structural transitions between vesicles and micelles are of great importance [5], for the reason that such phenomenon (micelle to vesicle transitions, MVT / vesicle to micelle transitions, VMT) offers an easy way of encapsulating active agents (like drug) by dissolving them in micellar solution prior to vesicle formation. This is important from both practical [6] and fundamental [7] points of view. Generally, MVT / VMT can be induced by changing the environemental factors like concentration [6*a*, 8], temperature [5*a*, 9], pH [10], light [11], CO_2 [12] or additive [13].

Most of the studies on MVT / VMT or vesicular structure formation deal with mixed cationic-anionic surfactant [5*a*, 14] systems becuase they can easily be form stable structures. Vesicle (or VMT) fomration in a single conventional cationic / anionic surfactant solution has rarely been found [8*c*, 10*c*, 15]. There are few reports available on MVT in an aqueous gemini surfactant or their mixtures under various experimental conditions (concentration, temprature or pH) [9*b*, 10*a* and *e*, 16]. However, mechanism of the MVT / VMT is yet to be settled [17].

Present chapter contains studies on the effect of different stimuli (e.g., concentration, pH, temperature and additive as organic and inorganic salts) on morphological transitions (MVT / VMT) in an aqueous isosorbide spacer based

cationic geimini surfactant (16-Isb-16) system using different techniques (DLS, ^{1}H NMR, Zeta (ζ) potential, fluorescence, TEM, POM, pH or condutometry). For morphological transitions, 16-Isb-16 has been selected as it has better physico-chemical (lower T_k, lower cmc and increased surface activity) and thermal properties over polymethylene spacer based geminis (for more details please see Chapter 3).

4.2. Materials and Methods

4.2.1. Materials

NaCl, NaSal and water were the same as used in Chapter 3. Sodium nitrate ($NaNO_3$, 99.80%, Merck), sodium bromide (NaBr, 99.50%, Sigma Aldrich), sodium hydroxide (NaOH, 99.50%, Merck), Chloroform ($CHCl_3$, 99.80%, Spectro-chem) and D_2O (99.9% atom **D**, Sigma Aldrich) were used as received. All the salts were dried in vacuum oven for 3–4 h before use. Buffer tablets (4, 7 and 9.2, Fisher-Scientific) are used to prepare buffer solutions of respective pH.

4.2.2. Methods

4.2.2.1. Sample Preparation

All the samples of 16-Isb-16 with and without salt are prepared in double distilled water using requisite amount of the surfactant (or salt). Samples with required pH were prepared by either using pH tablets or adjusted by addition of sodium hydroxide solution.

4.2.2.2. Dynamic Light Scattering (DLS) and Zeta (ζ) Potential Measurements

Dynamic light scattering measurements were performed with a Brookhaven 90 plus spectrometer equipped with in built temperature controller (± 0.5˚C). Light of λ of 633 nm (from 15 mW solid state He-Ne laser) was used as the incident beam. The scattering angle was 90˚ and the intensity autocorrelation functions were analyzed by using the methods of Cumulant and non-negatively constrained least-squares (NNLS) algorithm (software available with the instrument). The hydrodynamic diameter (D_h) was calculated according to Stokes-Einstein equation, $D_h = k_B T/(3\pi\eta D)$ where, D is diffusion coefficient, k_B is the Boltzmann constant, T is the absolute temperature, and η is the solvent viscosity. For particle size measurements, a 2.5 ml of surfactant solution of appropriate concentration was filtered through 0.22 μm nylon membrane filter to remove dust particle from the solution. Filtered solution was directly transferred into the 10 mm plastic cuvette (washed each time (before use) with fresh double distilled water to avoid dust particles). Sample cuvette was placed in the sample chamber after the initialization of the instrument (15 min.).The data obtained in each case are the average of 10 runs, each run of 30 s duration.

Zeta (ζ) - potential was also obtained by the DLS instrument at various temperatures. To obtain zeta and count rate data were fitted by the software using pH, particle size and concentration as fitting parameters. About 1.5 ml of surfactant solution was transferred into dipped (Uzgiris type) electrode plastic cuvette through nylon membrane filter (0.22 μm) and placed in a sample chamber. Data are average of 5 decay cycles (each decay cycle is of 5 runs with a 5 s interval).

4.2.2.3. ^{1}H NMR Measurements

^{1}H NMR measurements were recorded on the same Bruker spectrometer mentioned in previous Chapters. All gemini surfactant solutions were prepared in Deuterium oxide (D_2O). Each surfactant solution (0.6–0.7 ml) was transferred to a 5 mm NMR tube for measurements. In all experiments, numbers of scan was adjusted to achieve good signal to noise ratio.

4.2.2.4. Microscopy

Surfactant thin film was prepared by dissolving an appropriate amount of 16-Isb-16 in $CHCl_3$ and it stand overnight to evaporate the solvent. Traces of $CHCl_3$ were removed under high vacuum (5-10 mmHg) followed by dissolution in double distilled water. Solutions were gently mixed and then sonicated for 10-15 min. (at 30˚C).

Transition electron microscope (TEM) images were obtained with a Philip Tecnai 20 transmission electron microscope accelerating at a working voltage of 200 kV with CCD camera. A drop of gemini surfactant solution was placed on to the carbon-coated copper grid (200 mesh). Excess of water was blotted off with soft filter paper to form a thin film on the grid.

Polarizing optical microscope (POM) of Leica (DM2500) having differential interference contrast (DIC) lenses was also used for visualization of aggregates. Image was captured with an inbuilt Leica camera. Samples solution was applied on a Linkem heating chamber with quartz crucible. The Linkem chamber, with inbuilt heating sensor, was heated gradually (1°C / min) with the help of digital monitoring controller. The images with scale bar were obtained from the Leica software which is come inbuilt.

4.2.2.5. Fluorescence Measurement

Fluorescence measurements have been carried out with the same spectrophotometer (setup described in Chapter 3). However, slit widths of excitation and emission were fixed at 1.5 nm each and emission spectra were scanned between 350-600 nm at a scan rate of 60 $nm \cdot min^{-1}$.

4.2.2.6. pH Measurements

The pH measurement has been performed on calibrated digital Equip Tronics (EQ-614A) pH meter with an attached temperature controller.

4.2.2.7. Conductivity Measurements

For conductometry study, same conductivity meter was used which is already described in Chapter 3.

4.3. Results and Discussion

4.3.1. Effect of Concentration

Effect of [16-Isb-16] on morphological transitions has been studied using various techniques. The concentration of 16-Isb-16 was varied from 0.005 to 20 mM. The most dramatic changes are observed between 1 and 5 mM.

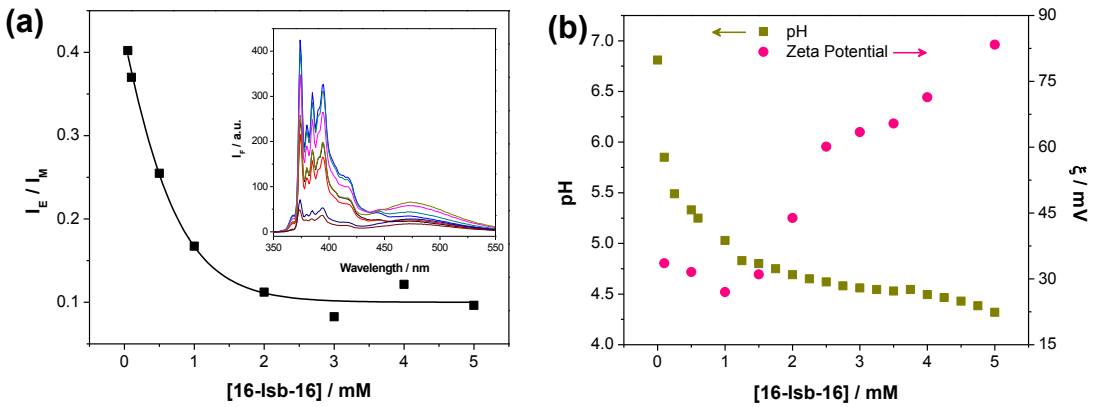

Figure 1. (*a*) Ratio of the intensities of excimer to monomer (I_E/I_M) of pyrene and (*b*) pH and zeta (ζ)-potential variation with [16-Isb-16].

Variation of the ratio of fluorescence intensities of the excimer to the monomer (I_E/I_M) with [16-Isb-16] (from ~0.5 to 5 mM) has been shown in Figure 1*a*. It can be seen that the above ratio increases on dilution. It may be due to s decrease in number density of the micelle in the solution. The number density can decrease either due to less amount of 16-Isb-16 or due to growth in micelle size (which require more monomers). However, this was not clarified from Figure 1*a*.

^{1}H NMR has been used to get an idea about the environmental change of different protons during the aggregation process as well as micellar morphological transition [18]. From Figure 2, one can see that changes of proton chemical shift with decrease in [16-Isb-16] do not follow a regular transition profile. Interestingly, proton of $-N^+(CH_3)_2$ shows splitting and shifting towards up field at lower concentration (1 mM). It may be due to the presence of $-N^+(CH_3)_2$ groups in two different

environments hinting towards the coexistence of two different morphologies in the solution [19]. If vesicles are present with the micelles in the sample, they cannot exchange fast with each other because of the stability of the former leading to a signal splitting [15, 20].

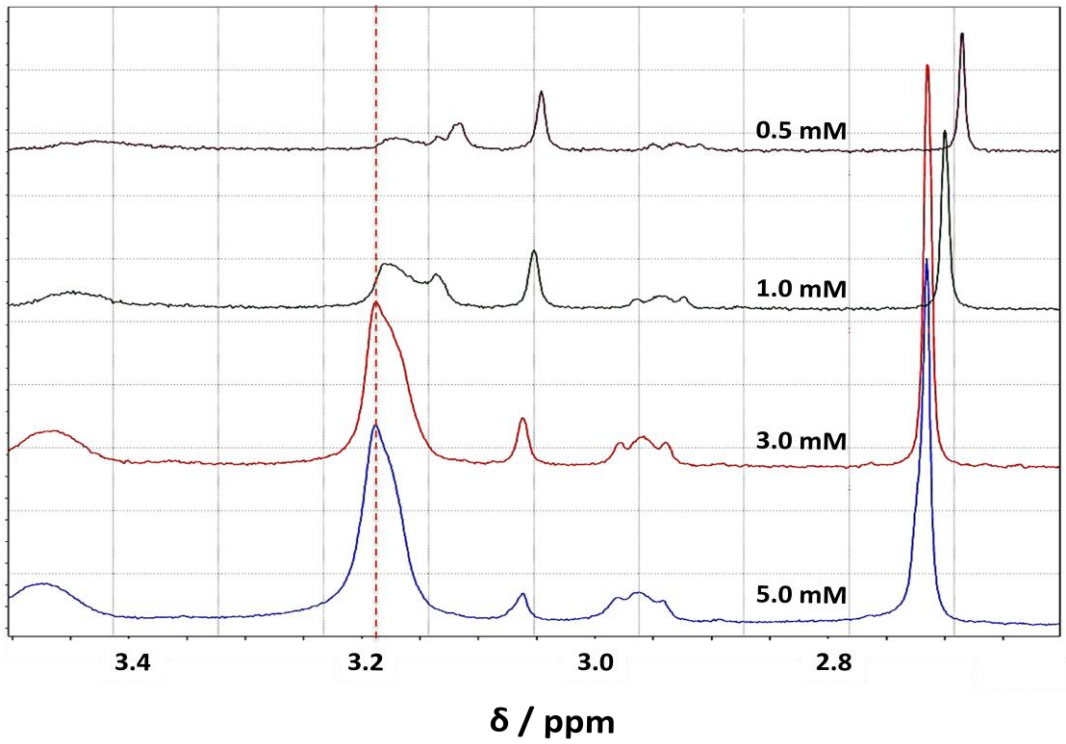

Figure 2. Part of ^{1}H NMR spectrum of 16-Isb-16 as a function of concentration in D_2O. Highlighted portion of NMR spectra showing the splitting of $-N^{+}(CH_3)_2$ peak at lower concentration.

The fluorescence and NMR studies hint about the morphological transition upon dilution. To further investigate the process, DLS studies are performed to measure the size of the aggregate at different concentrations of the 16-Isb-16 (Figure 3*a*). Aggregates have an average hydrodynamic diameter ($\langle D_h \rangle$) of 3.9 nm with narrow bimodal size distribution (SD) at 5 mM of 16-Isb-16 with low polydispersity index (PI = 0.193, calculated by the Cumulant method). The low PI value indicates that micelles are the dominant aggregates in the system (Figure 3*b*). PI grew from 0.193 (5 mM) to 0.466 (3 mM), which is indicative of the increase in the vesicle

micelle ratio in the system on dilution [21]. However, the PI value again decreases to 0.223 (1 mM) indicating again of the predominance of one type of aggregates in the solution. It should be mentioned here that PI values are high, and, therefore, the meaning of D_h is not state forward [22]. The variation of relative scattering intensity against the diameter of the 16-Isb-16 aggregates (D_h) shown in Figure 3. At 5 mM 16-Isb-16, two small size distributions at ~1 nm and ~20 nm co-exist. When the 16-Isb-16 concentration decreases (3 mM), the two distributions change significantly (~5 nm and ~200 nm). On further dilution (1 mM), a single broad SD of large size (~400 nm) appears. DLS data show a morphological transition which is initiated by only dilution. Since DLS does not give the aggregates size directly but the diffusion coefficient (strong micellar attraction can result a large size and *vice-versa*) [18].

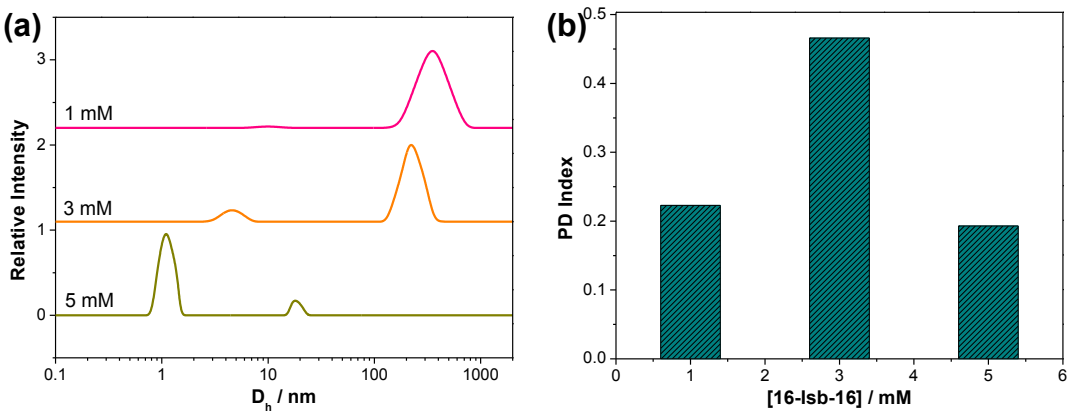

Figure 3. (*a*) Apparent hydrodynamic diameter (D_h) distributions; (*b*) Polydispersity (PD) Index of aggregates formed in the aqueous solution of 16-Isb-16 at different concentrations.

The size information has been collected by TEM measurements (Figure 4). The aggregate morphologies are obviously different at different concentrations. At 5 mM, small aggregates are observed, which is consistent with low PI values obtained from DLS measurements (Figure 3*b*). The data show the presence of micelles with a few bigger aggregates. At 2 mM of 16-Isb-16, most of the aggregates were in the fused states. The fused aggregates transfer to large spherical aggregates at 1 mM 16-

Isb-16. These aggregates are well separated and vesicular in nature (vesicles). The unique morphological transition takes place by adding simple solvent water (dilution). The presence of vesicles in 1 mM sample was even seen by a polarizing optical microscope (Figure 4*e*). However, we were failed in our attempt to see aggregates for other concentrations by POM.

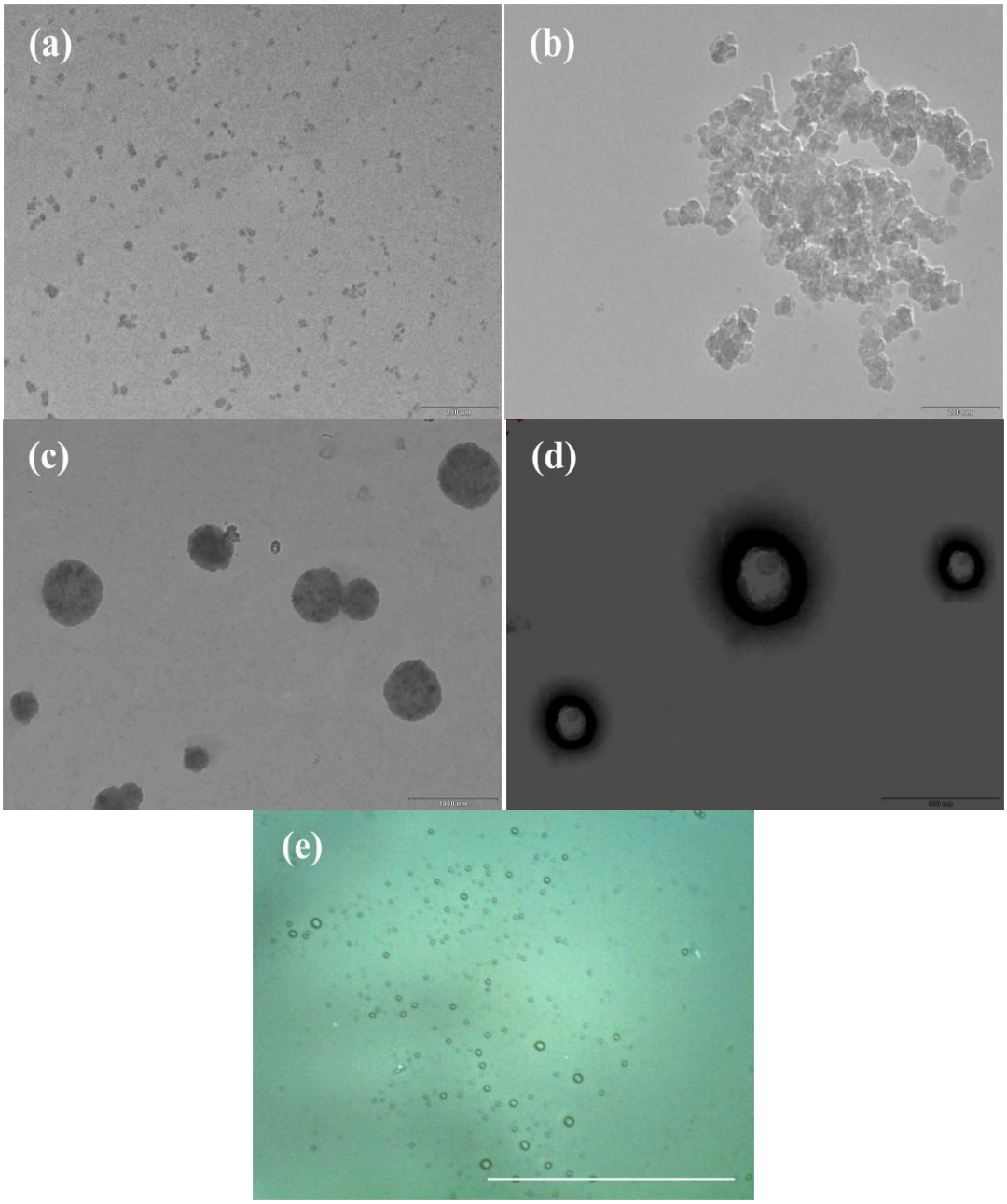

Figure 4. TEM images: (*a*) 5 mM; (*b*) 2 mM; (*c*) 1 mM; (*d*) 1 mM (with negative stained of uranyl acetate solution for 10-15 sec) and (*e*) POM images 1 mM of aqueous solution of 16- Isb-16 at 25°C. Scale bar represents: (*a*) 0.2 µm; (*b*) 0.2 µm; (*c*) 1 µm; (*d*) 0.5 µm; (*e*) 50 µm, respectively.

Spontaneous vesicle growth could, in principle, occur either gradually by the incorporation of monomer to the vesicles or by a step-wise fusion process with other vesicles (Scheme 1). Gradual growth is possible if the rate of incorporation of monomer into pre-existing vesicles is greater than rate of spontaneous assembly into new vesicles. It has been reported that pH can play an important role in all above transitions. Figure 2*b* shows the variation of pH of 16-Isb-16 solution on dilution. Looking at Figure 2*b* and 4, it is clear that micelles exist at low pH (5 mM) while vesicles exist at higher pH (1 mM). A workable mechanism for these effects is given in following paragraphs.

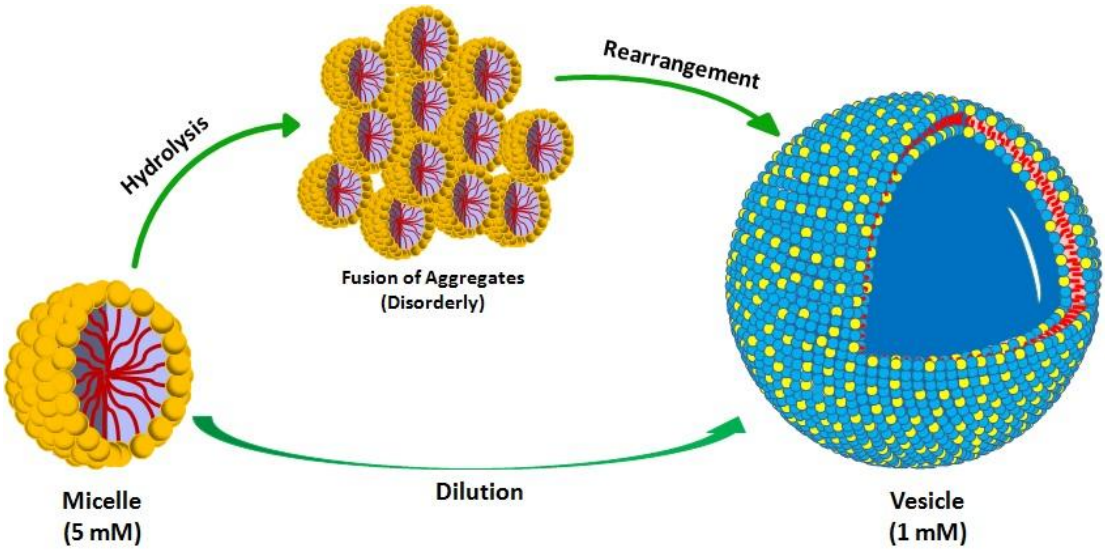

Scheme 1. Schematic representation of dilution induced micelle to vesicle transition in single aqueous isosorbide spacer based cationic gemini surfactant (16-Isb-16.)

The 16-Isb-16 ($(RSN_2)^{+2}2Cl^{-}$, R represents both alkyl chains, S represents spacer and N_2 represents two nitrogen atoms molecule being salt of strong acid and weak base can get hydrolyze [17] in water according to the reaction

$$(RSN_2)^{+2}\cdot 2Cl^{-} + 2H_2O \Leftrightarrow (RSN_2)^{+2}\cdot 2OH^{-} + 2HCl$$

This is indicated by pH (4.3) in concentrated 5 mM 16-Isb-16 solution (Figure

1*b*). At higher concentration, the degree of hydrolysis of above surfactant would be smaller. Therefore, the ratio of ionized form of salt to that of hydrolyzed form of salt will be high and is responsible for higher repulsion between surfactant head groups with a concomitant breaking of hydrogen bonding between ester groups of the spacers. These factors seem responsible for spherical micelle in the solution (Figure 4*a*). With the decrease in 16-Isb-16 concentration, the degree of salt hydrolysis increases. Therefore, base form of surfactant (weak base) is expected relatively more in a typical micelle. Hence, charge on the head group will be shielded due to the presence of solubilized weak base. The idea of lower charge on the micelle finds support from our zeta potential data depicted in Figure 1*b*. The closer head group approach may also facilitate the hydrogen bonding in the spacer. Since charge on the aggregate is depleting, aggregates have less objection to come near to each other and can fuse. This indeed was observed in Figure 4*b*. The above approach may also stabilize various intra and inter molecular hydrogen bonding in the aggregates and responsible for bigger vesicles in the solution (Figure 4*c*-*e*).

4.3.2. Effect of pH

It has been seen that pH play an important role in dilution induced morphological transition of 16-Isb-16 by neutralizing the ammonium head groups. To understand the phenomenon, pH variation has been done (using different buffers) at a fixed [16-Isb-16] (Figure 5).

Structural transition in 16-Isb-16 solution, with pH (NaOH used to vary the pH) is studied by DLS (Figure 5*a* and *b*). Two 16-Isb-16 concentrations (5 mM, micellar and 1 mM, vesicular) are used for the morphological variations (Figure 5).

For 1 mM 16-Isb-16 (Figure 5*b*) at 6.16 pH (without pH adjustment), a broad bimodal SD with most vesicular region (hydrodynamic diameter (D_h) ~200-700 nm) has been observed. The polydispersity index (PDI) with the value of 0.286 was also supporting for the presence of mono disperses aggregates (Figure 5*c*). As the pH increases to 7.00, the vesicular region decreases and micellar region crop up with an increase in PDI value 0.58. However, vesicular region is still in dominant phase.

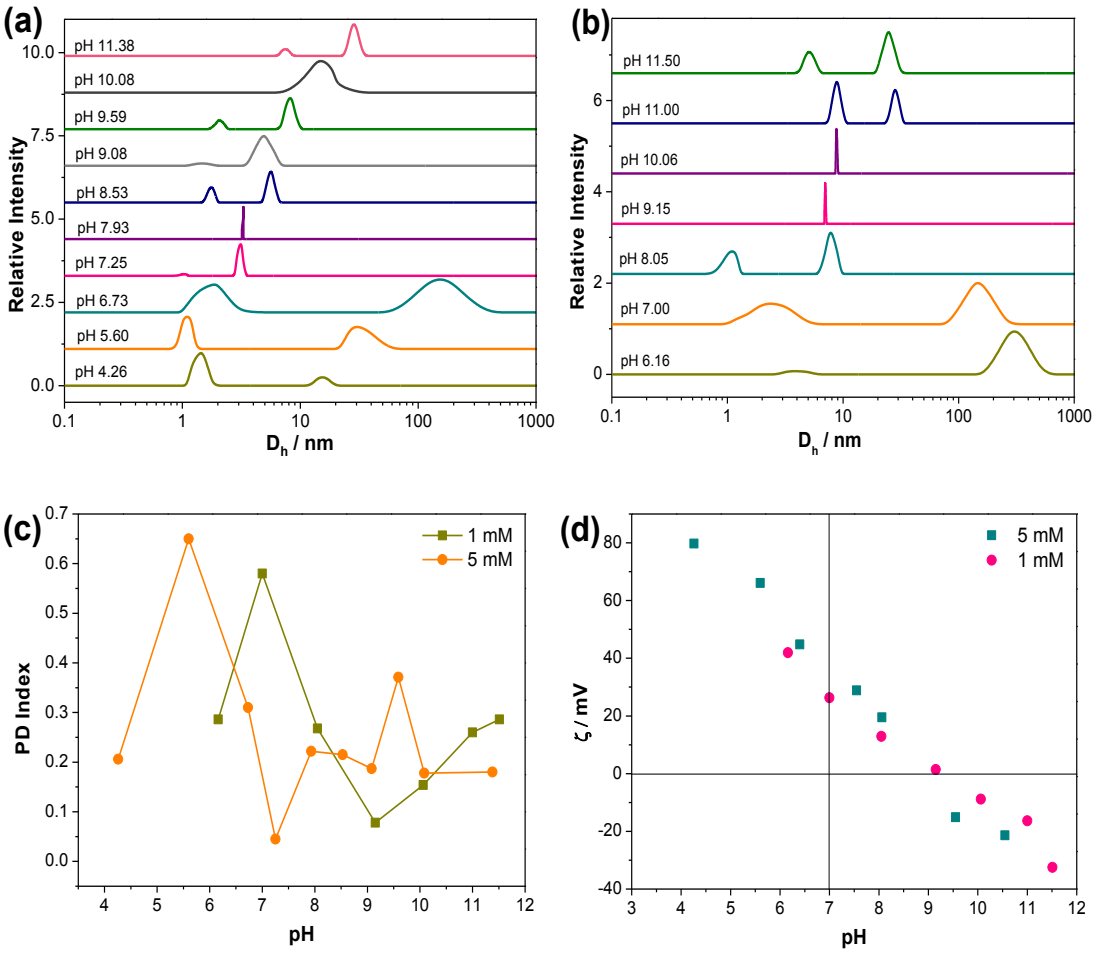

Figure 5. pH mediated particle size distribution (5 mM (*a*) and 1 mM (*b*)), polydispersity (PD) index (*c*) and Zeta (ζ) potential (*d*) of 16-Isb-16 at 25°C.

Interestingly, as passes from the neutral to the basic pH (9.15), the aggregates were transferred into micelles with a lower PDI (0.078) indicating the narrow monomodal SD with the D_h of ~8-10 nm. The monomodal SD converted to the biomodal as further increased in the pH from 9.15 to 11.50 but the aggregates size and

PDI was not that much changed (Figure 5*c*). For 5 mM 16-Isb-16 at wide range (4.26 to 11.38) of pH (Figure 5), same results have been obtained, where, vesicular region have been obtained at 6.73 pH.

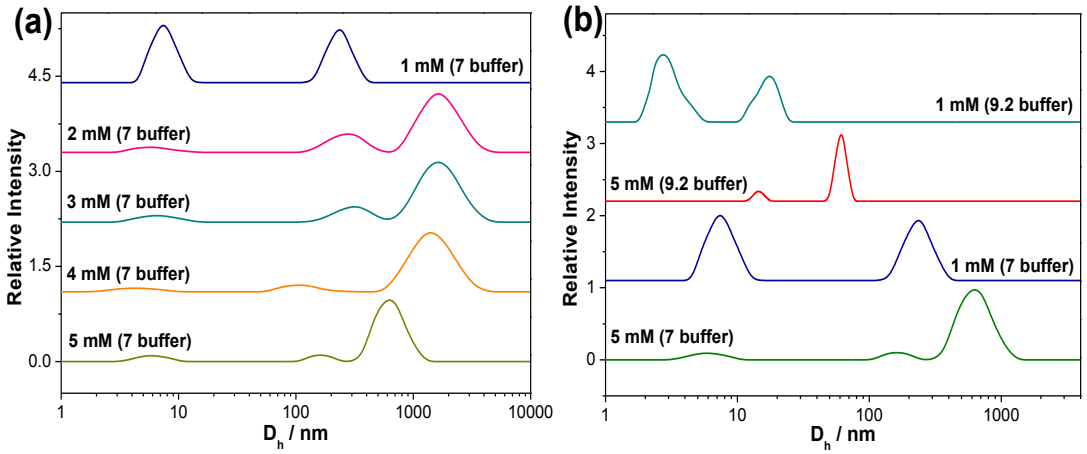

Figure 6. D_h of 16-Isb-16 solution at 25°C: (*a*) different concentrations (5 to 1 mM) at fixed 7.0 pH; (*b*) 5 and 1 mM (in 7 and 9.2 buffer solution).

DLS of 16-Isb-16 at concentrations of 5 to 1 mM has also been performed at fixed 7.0 buffer solution (Figure 6*a*). The result clearly indicates that the formation of vesicles obtained is possible with other concentrations of 16-Isb-16 at fixed 7.0 pH. Hence, pH can be a vital stimulus for the formation of vesicles. However, dilution with water is also responsible for the change and the results (Figure 3*a*). pH also varied from 7 to 9.2 in 5 and 1 mM 16-Isb-16 solutions (Figure 6*b*). Similar results (lower size of aggregates at basic pH) have been obtained for the both buffer solutions.

Zeta (ζ) – potential measurement (Figure 5*d*) has also been performed to understand the morphological transitions (as well as vesicle formation) at neutral pH of 16-Isb-16. For both the concentrations (5 and 1 mM), ζ decreases linearly (with good correlation) as the pH increases (from 4 to 11.5). 16-Isb-16 was present in its original form of $S^{2+}X$ (cationic form) with positive surface charged density at 6 pH. The concentration of $S^{2+}X$ form of 16-Isb-16 decreases and SOH (neutral form)

concentration increases when pH of the solution is increased from 6 to 7.5. This is also reflected in decrease of surface charge of the aggregates (40 to 20 mV). However, it has been shown that 1mM 16-Isb-16 (with the same ζ) forms vesicles in solution. Similarly, at neutral pH (6.5-7), equilibrium may be exist between $S^{2+}X$ and SOH types of the surfactant (with lower surface density) which is responsible for the electrostatic attraction and resulting into vesicle formation. SOH form of 16-Isb-16 can decrease the hydrogen bonding interaction between surfactant and water molecules and may responsible for the vesicle formation (due to internal interaction of within the aggregate). However, due to the presence of $S^{2+}X$, micelle are also present in the system (as confirmed by DLS data, Figure 5*a* and *b*).

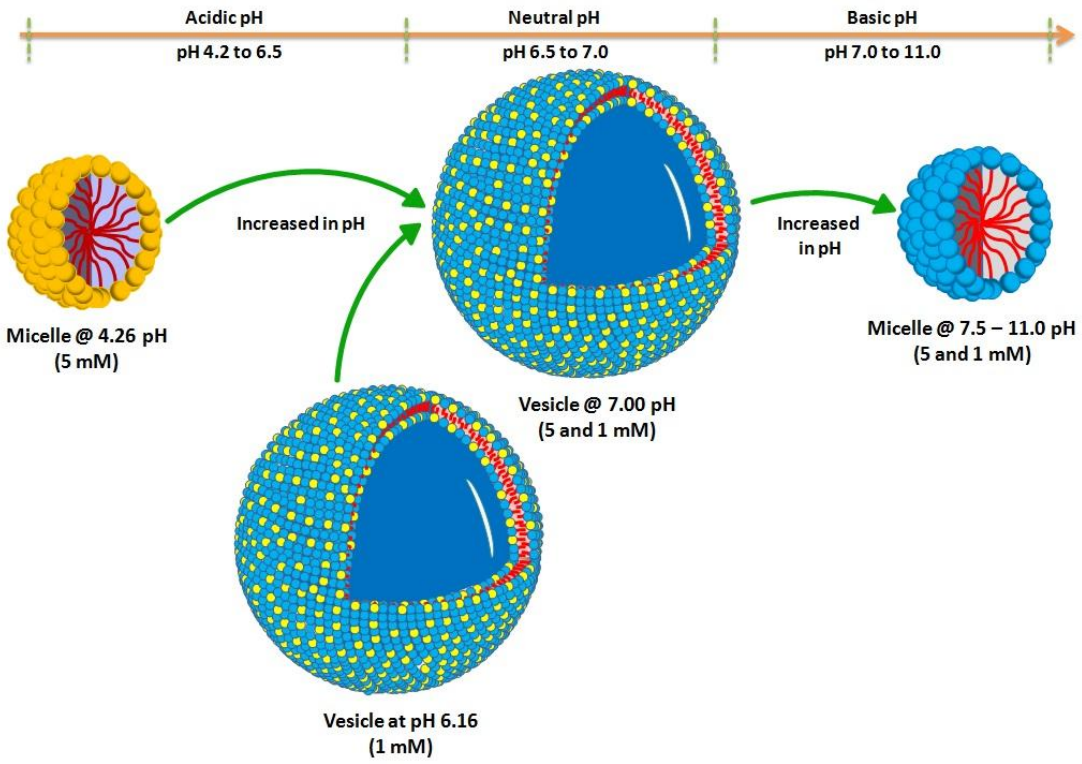

Scheme 2. Schematic Representation of pH induced micelle to vesicle transitions in 16-Isb-16.

As pH increase (from 7 to 8.5) ζ decreases from 20-25 to 0. This is the indication of complete neutralization of 16-Isb-16 aggregates. At this stage (From DLS results), the vesicles are converted into micelles. According to DLVO theory

[14*d*], surface charge at low density, aggregates / vesicles should be colloidally unstable (where the attractive van der Waals interactions dominate). Further, increase in the pH (from 8.5 to 11.5), surface charged density becomes completely negative indicating the SOH^{2-} (anionic form) type of surfactant which may produce negatively charged micelles with no significant changed in the D_h (~2-25 nm) (Figure 5*a* and *b*). Thus, pH (pure / buffer controlled) is a key stimulus responsible for MVT or VMT (Scheme 2).

4.3.3. Effect of Temperature

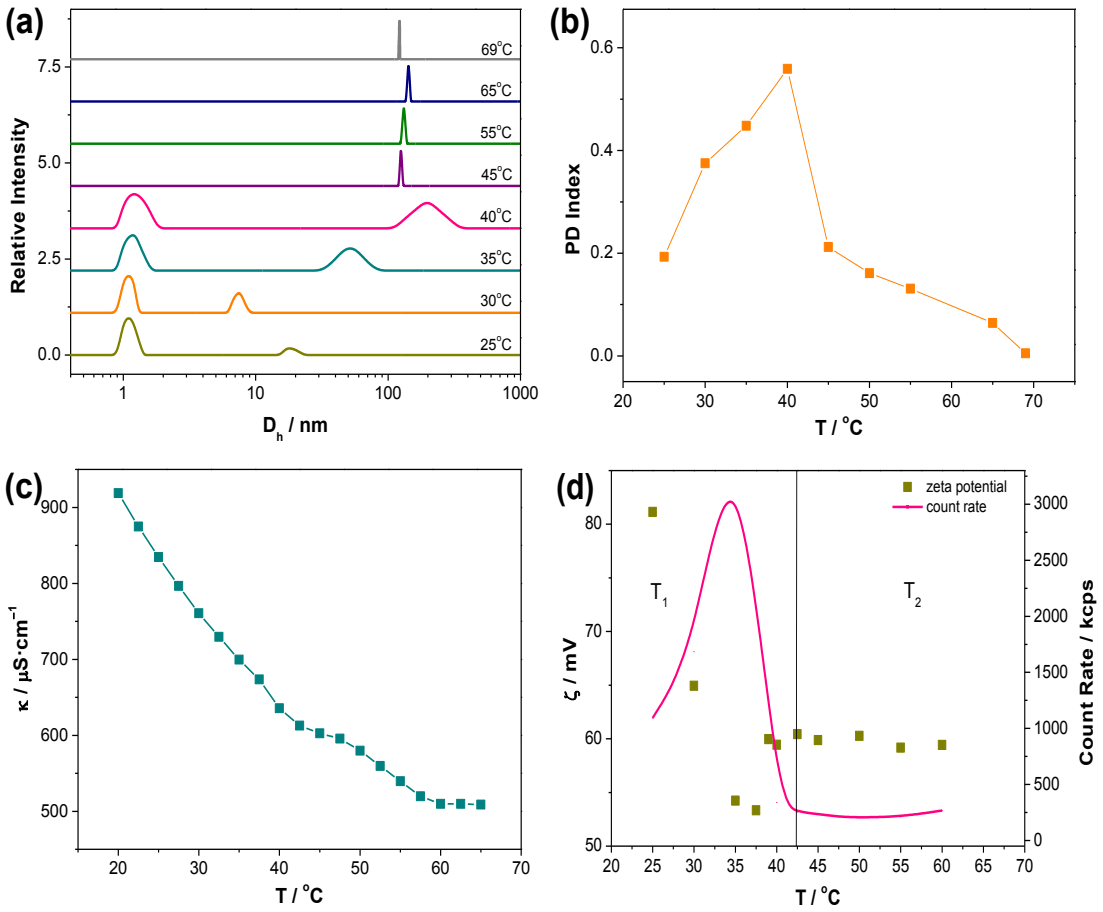

Figure 7. (*a*) Particle size distributions; (*b*) polydispersity (PD) index; (*c*) variation of specific conductance (κ); (*d*) zeta potential (ζ) and count rate of 5 mM 16-Isb-16 at different temperatures (*T*, 25 – 70°C).

Temperature induced MVT has been observed in aqueous solution of 5 mM 16-Isb-16. However, no morphological changes are observed in 1 mM 16-Isb-16 with temperature. Micelles are formed in the 5 mM aqueous solution of 16-Isb-16, which is already verified by TEM (Figure 4). Therefore, the changes (from micelle to vesicle) have been examined by the DLS within the temperature range of 25-70°C (Figure 7*a*). Figure 7*a* shows that micelle is the dominant morphology at 25°C. The lower PDI value (0.193) confirms the presence of mono disperse aggregate (Figure 7*b*). When the temperature of the sample was increased (25 to 40°C), aggregate size (~1-10 nm) was dramatically changed to the morphology of ~100-500 nm with a broad bimodal SD (Figure 7*a*). On further increase in the temperature (from 40 to 70°C), aggregates with D_h ~100-200nm were remained stable and bimodal SD were also converted into monomodal SD. The PDI values are also confirming the morphological transition (0.559 at ~40°C) and larger aggregates / vesicle formation (~0.005-0.212 above 40°C).

To understand the phenomenon, this transition has also been examined by conductivity measurements (Figure 7*c*). Figure 7*c* demonstrates that conductance decreases as the temperature increases (from 25 to 70°C), which is consonance to a recent study [23]. Conductivity basically depends on mobility of the free ions in the solution [24]. The higher (at 25°C) and lower (at 70°C) value of conductance denote the presence of more and less free ions in the solution, respectively. Less free ions (without any buffer) clearly indicate the presence of lower curvature aggregates (i.e., vesicle / bilayer). However, a little break point in conductance *vs T* plot (40-45°C) has also been observed which may be due to the structural transition.

These observations find support from the count rate and zeta (ζ) - potential data as a function of temperature (Figure 7*d*). The clear transition has been observed

at ~ 42.5°C. Similar transition (MVT) has been observe where count rate increases up to certain value (1000-3000 kcps) and then decreases (3000-300 kcps) as the temperature increases (25 to 40°C) then followed by a near constancy (~250-300 kcps) as the temperature increases further (40-60°C). This indicates that the spherical micelles may fused together and form larger aggregates / vesicles and responsible for count rate decreases [25]. Moreover, ζ values also showing similar kind of results (but the trend was a little bit different). ζ decreases (from 80 to 55 mV) and then remains constant (57-60 mV) as the temperature increases (25-60°C). In aqueous solution, 16-Isb-16 mainly present in the form of $S^{2+}X$ (cationic) at room temperature (25°C), confirmed by higher positive surface charge (+ve zeta potential). Temperature increases surface charge of the aggregate decreases. This may be due to two reasons: (a) breaking of intra- / inter- molecular H-bonding of water molecule at air-water interface; (b) bound Cl^- are replaced by OH^- [26]. Therefore, surface charge density clearly showed the transfer from cationic to nonionic (SOH) or mixture of cationic and nonionic which is responsible for electrostatic attraction (counter-ion binding) and resulting into formation of vesicle at higher temperature. This was further confirmed by ^{1}H NMR.

^{1}H NMR spectra with $–N^+(CH_3)_2$ peak (located at the air-water interface) for 5 mM 16-Isb-16 (in D_2O) are shown in Figure 8. The main observation from the Figure 8, is the downfield shift of the $–N^+(CH_3)_2$ peak (from 25-70°C). This may be due to dehydration of the head group region of the surfactant aggregates [27] which is confirming the preposition made from zeta potential results. Another observation is the splitting of the signal at higher temperature (40°C). It may be due to the presence of $–N^+(CH_3)_2$ groups in two different environments hinting towards the coexistence of two different morphologies in the solution [19]. If vesicle present with the micelle in

the sample, they cannot exchange fast with each other because of long-term stability of the former, leading to signal splitting [15, 20]. Similar kind of changes has also been observed with other peaks too.

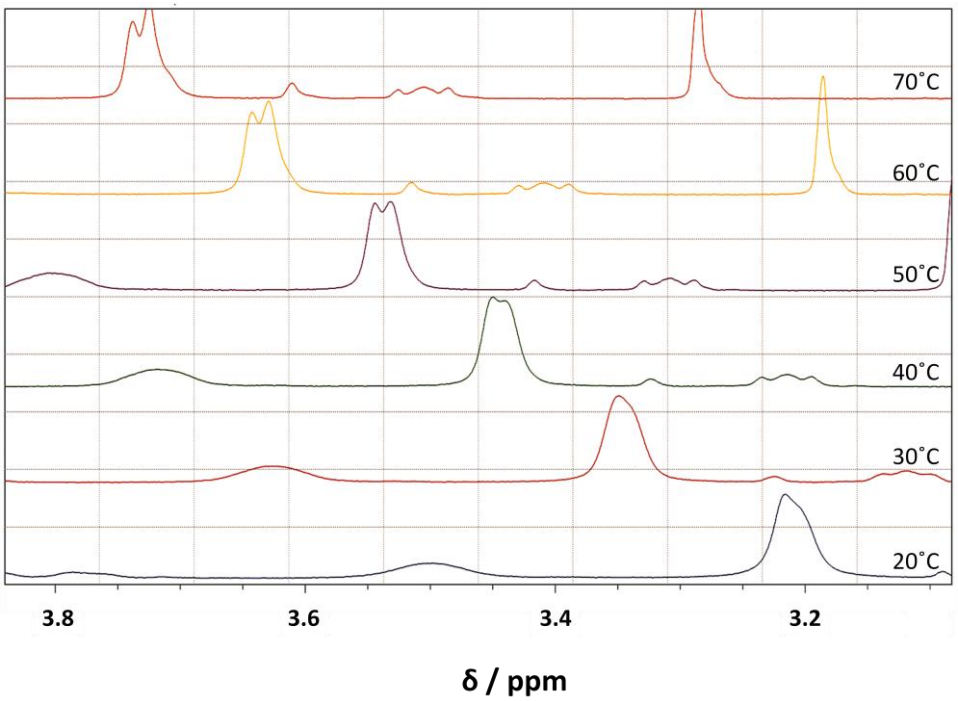

Figure 8. ^{1}H NMR spectra with particular $-N^{+}(CH_3)_2$ peak of 16-Isb-16 at 5 mM concentration with different temperatures in D_2O.

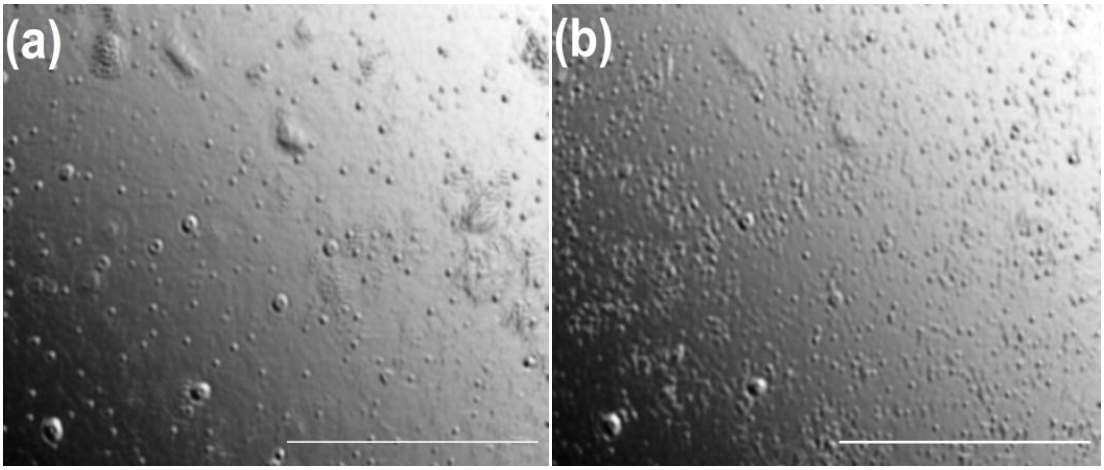

Figure 9. Polarizing optical microscope (POM) images of 5 mM 16-Isb-16 at (*a*) 43°C and (*b*) 47°C. Scale bar represents 20 µm.

Above data prompted us to investigate the morphological transition (MVT) by optical microscopy. Figure 9 shows the presence of vesicular aggregates (vesicles)

with 5 mM 16-Isb-16 (at 43°C and 47°C). The sizes are quite comparable with DLS results (Figure 7*a*). However, number of aggregates was higher in case of 47°C. This may be due to the transition (from micelles to vesicle). Hence, it can be concluded by visual observation (and NMR) that spherical micelles converting into vesicles with increasing temperature (scheme 3).

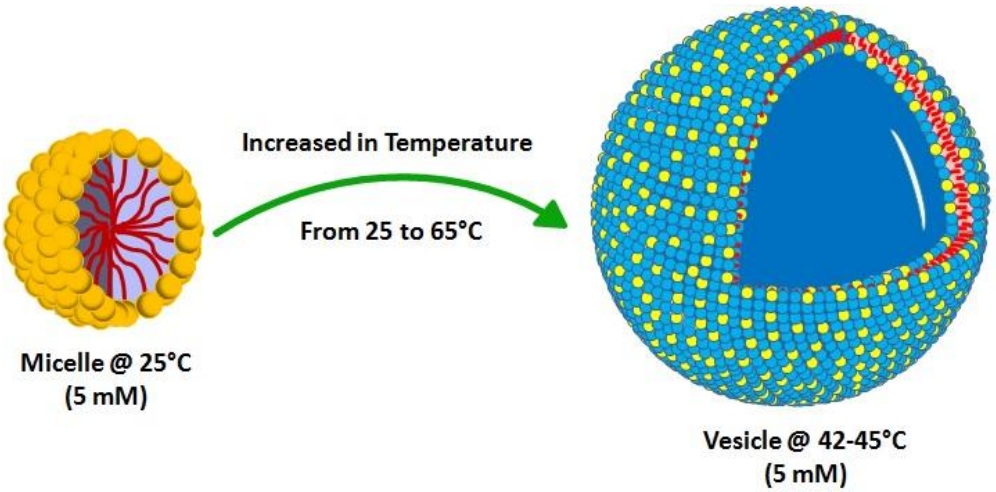

Scheme 3. Schematic Representation of temperature induced micelle to vesicle transition in 16-Isb-16.

4.3.4. Effect of Salt

Various anions (in a role of counter-ion) have been added to see the morphological transition (vesicle to micelle transition, VMT) by varying the concentration of inorganic as well as organic salts (NaCl, NaBr, $NaNO_3$ and NaSal) in aqueous solution of 1 mM 16-Isb-16 (fixed) at 25°C. Vesicles were the major aggregates in the 1 mM aqueous solution of 16-Isb-16 (as already verified by TEM, Figure 3 and DLS results, Figure 2*b*). To understand the effect of salts, DLS measurements are performed (Figure 10). Once again, DLS data clearly show the presence of vesicles in 1 mM aqueous solution of 16-Isb-16 (monomodal SD, D_h ~200-500 nm) with relatively lower (~0.2) PDI value (Figure 11). From Figure 10, it

can be observed that monomodal SD (vesicle) is converting into broad bimodal SD with a D_h ~5-10 nm (micelle) and ~200-600 nm (vesicle) with the addition of salt (NaCl, NaBr, $NaNO_3$ or NaSal). The higher PDI values (0.35-0.8) support the conversion of vesicles into micelles.

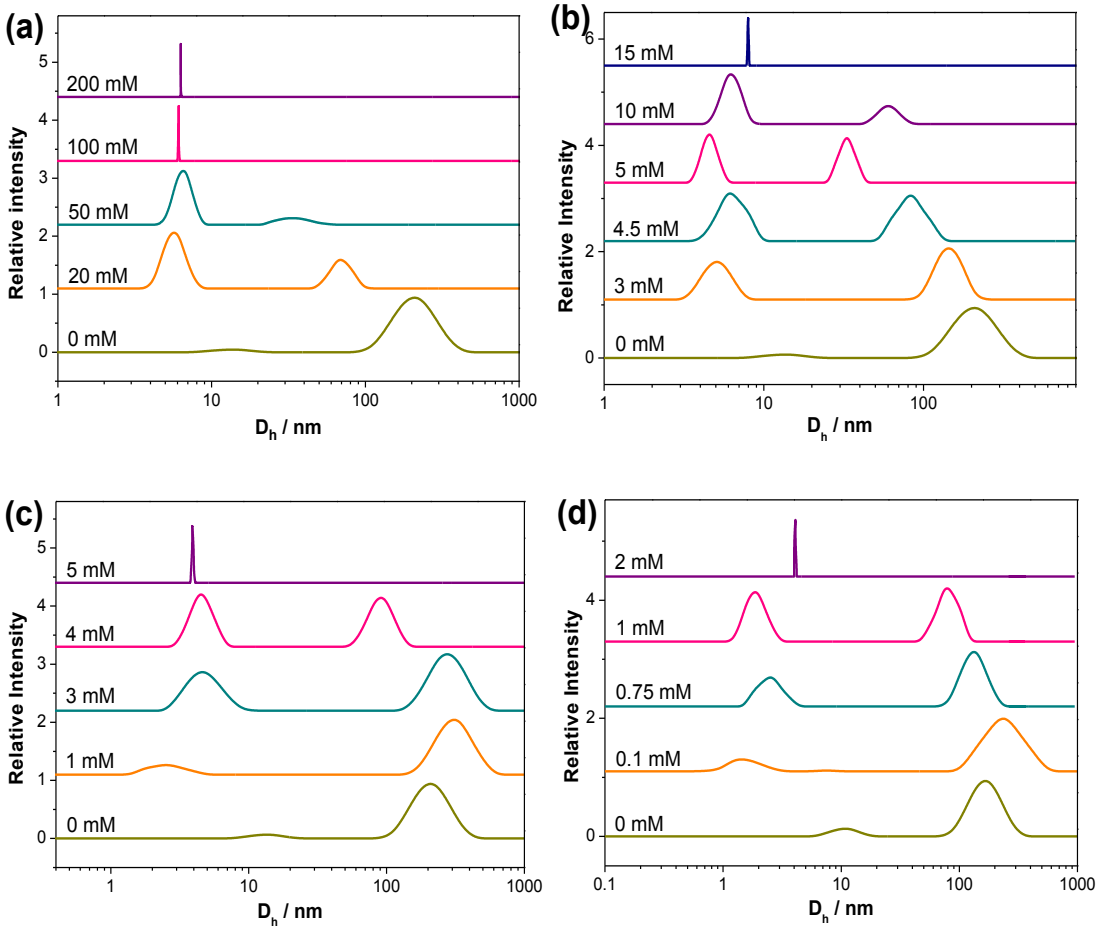

Figure 10. Particle size distribution of 1 mM 16-Isb-16 with different concentration of salts: (*a*) NaCl; (*b*) NaBr; (*c*) $NaNO_3$; (*d*) NaSal.

With further increase of [salt], broad bimodal SD converted into narrow monomdal SD with a D_h ~3-8 nm with relatively lower PDI value (~0.05-0.2). This indicates complete conversion into micellar structure. However, the concentration required for VMT was different for each sodium salt. This indicates the role of anion specificity. For instance, a large amount of NaCl (75-100 mM) was required for transition whereas NaSal was needed only 1-2 mM. It allows following order of the

anions according to the requirements of the salt for VMT, $Sal^- < Br^- < NO_3^- < Cl^-$. Similar ordering of anions was also observed for polydispersity index (Figure 11*a-d*). This ordering (Figure 11*e*) was found in good agreement with the classical Hofmeister like series [28].

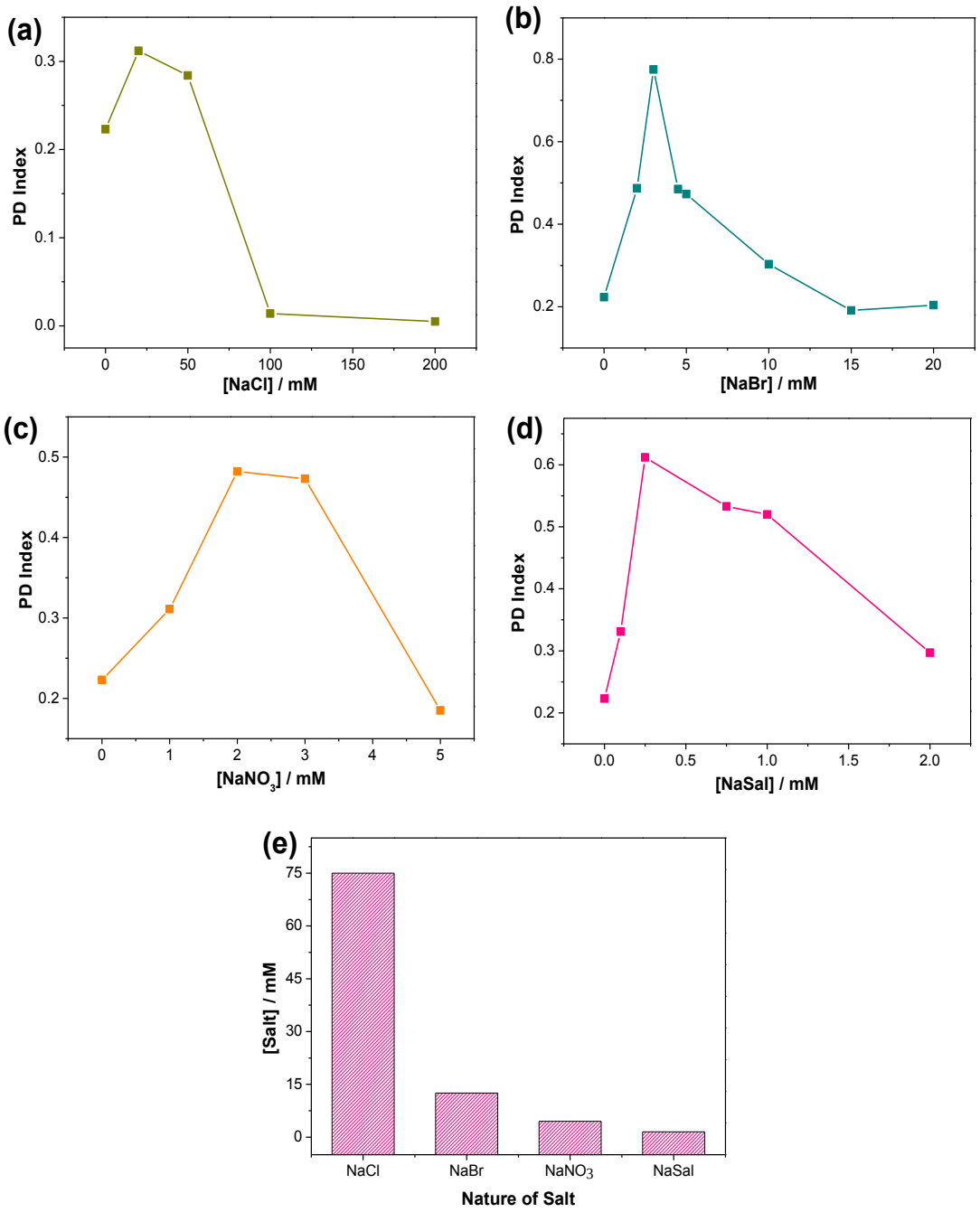

Figure 11. Plot of Polydispersity (PD) index *vs* [Salt] of 1 mM 16-Isb-16 at 25°C: (*a*) NaCl; (*b*) NaBr; (*c*) $NaNO_3$; (*d*) NaSal. (*e*) Plot of observed [salt] for VMT *vs* nature of salt in 1 mM aqueous solution of 16-Isb-16 at 25°C

In the last decade, salt induced VMT in single surfactant system has been reported [8*c*, 9*b*, 13*e*]. With the help of the earlier interpretation, a working mechanism for VMT in the present case is proposed: a weakening of electrostatic attraction between $S^{2+}X$ (cationic) and / or SOH (neutral) types of surfactant monomer in presence of salt are expected. The order of counter-ion binding plays an important role. The addition of any salt / anion (Cl^- / Br^- / NO_3^- / Sal^-) would bind to the gemini species (meanwhile will replace the OH^-) and probably decrease in the attraction (inter- / intra-molecular H-bonding) between head groups / spacer, resulting into a breakdown of bilayer / vesicle structure (Scheme 4) [29].

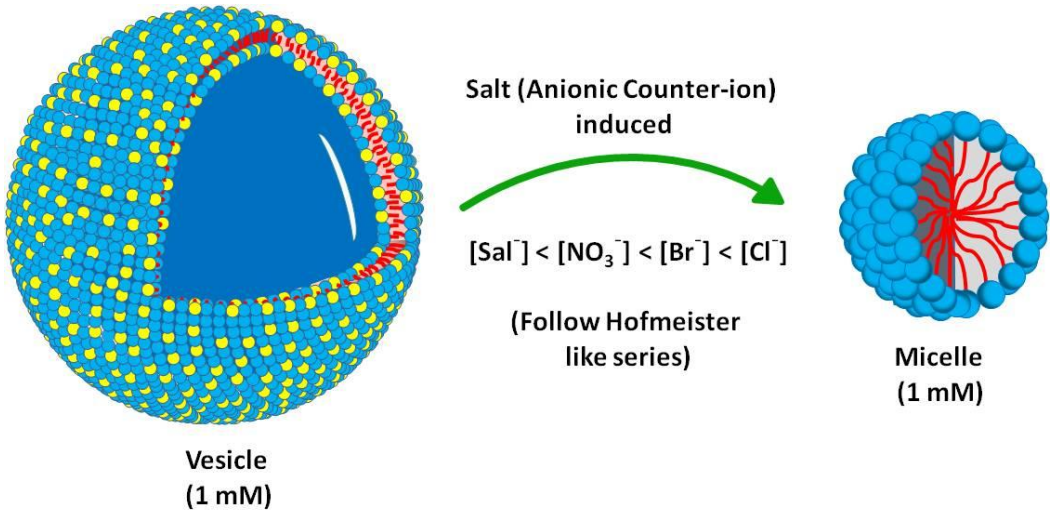

Scheme 4. Schematic Representation of salt (anionic counter-ion) induced Vesicle to micelle transition in 1 mM 16-Isb-16 aqueous solution.

NaCl concentration required for VMT is five times higher than of NaBr. NaBr and $NaNO_3$ concentrations are not much different. However, NaSal concentration required is fifteen and seventy five times lower than the NaCl and NaBr, respectively (Figure 11*e*). This is because of difference in order of counter-ion binding to the surfactant aggregates.

4.4. Conclusion

Stimuli responsive (concentration (dilution), pH, temperature and nature of salt) morphological transitions (micelle to vesicle / vesicle to micelle transition) has been shown in a single aqueous isosorbide (sugar) spacer based cationic gemini surfactant (16-Isb-16, Scheme 5).

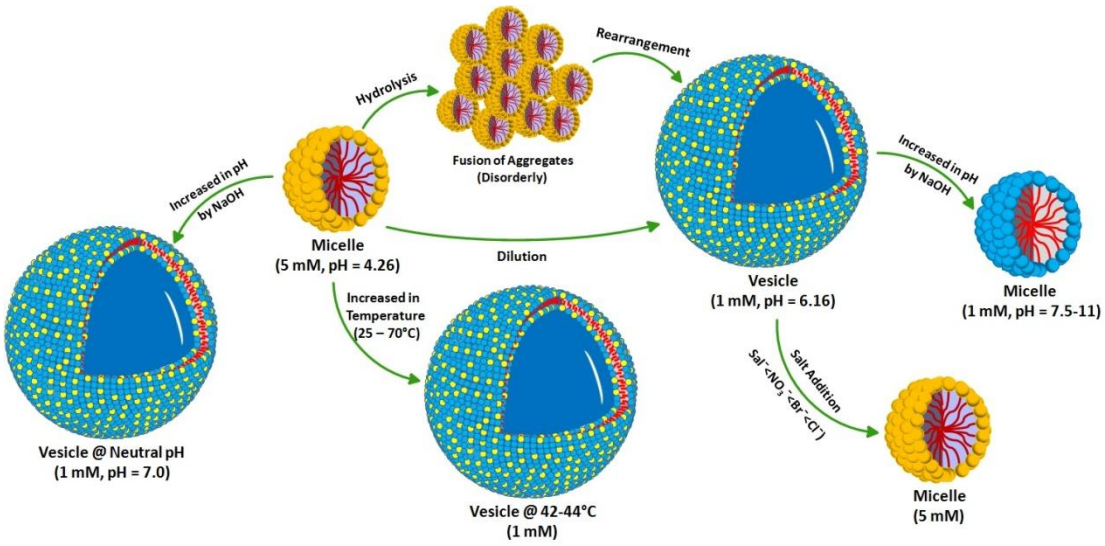

Scheme 5. Stimuli responsive micelle to vesicle to micelle transitions in single cationic gemini surfactant aqueous system.

Fusion of smaller spherical aggregates with electrostatic attraction at neutral pH, cleavage of H-bonding (inter- / intra-molecular) and / or role of counter-ions seems to be the major driving force(s) for the so called morphological transitions. Reproducibility as well as reversibility was observed for the similar sample and transitions were found remarkably distinct. This work may find application in the field of controlled drug release as well as in biological studies [30].

References

[1] M. Rosoff, Marcel Dekker, Surfactant science series 62; Vesicles, ed. Inc., New York, 1995.

[2] R. Lipowsky, R. Sackmann, Handbook of Biological Physics, ed., Elsevier, Amsterdam, 1995.

[3] D. D. Lasic, *Angew. Chem. Int. Ed.* 106 (1994) 1765.

[4] I. Yaacob, A. C. Nunes and A. Bose, *J. Colloid Interface Sci.* 171 (1995) 73.

[5] (*a*) H. Yin, Z. Zhou, J. Huang, R. Zhang, Y. Zhang, *Angew. Chem. Int. Ed.* 42 (2003) 2188; (*b*) L. Jiang, K. Wang, F. Ke, D. Liang, J. Huang, *Soft Matter* 5 (2009) 599.

[6] (*a*) M. J. Russell, *Science* 302 (2003) 580; (*b*) J. S. Martinez, G. P. Zhang, P. D. Holt, H. T. Jung, C. J. Carrano, M. G. haygood, A. Butler, *Science* 287 (2000) 1245.

[7] (*a*) M. Martin, S. M. Hanczyc, J. W. Szostak, *Science* 302 (2003) 618; (*b*) S. Laurent, D. Forge, M. Port, A. Roch, C. Robic, L. V. Elst, R. N. Muller, *Chem. Rev.* 108 (2008) 2064.

[8] (*a*) Z. Hu, A. M. Jonas, S. K. Varshney, J-F. Gohy, *J. Am. Chem. Soc.* 127 (2005) 6526; (*b*) A. E. Speers, C. C. Wu, *Chem. Rev.* 107 (2007) 3687; (*c*) A. Mohanty, T. Patra, J. Dey, *J. Phys. Chem. B* 111 (2007) 7155; (*d*) G. Verma, V. K. Aswal, G. Fritz-Popovski, C. P. Shah, M. Kumar, P. A. Hasan, *J. Colloid Interface Sci.* 359 (2011) 163.

[9] (*a*) H. Q. Yin, S. Lei, S. Zhu, J. B. huang, J. P. Ye, *Chem. Eur. J.* 12 (2006) 2825; (*b*) S. J. Ryanen, V. M. J. Saily, M. J. Parry, P. Luciani, G. Mancini, J-M. I. Alakoskela, P. K. J. Kinnunen, *J. Am. Chem. Soc.* 128 (2006) 8659; (*c*) S. Y. Kim, K. E. Lee, S. S. Han, B. Jeong, *J. Phys. Chem.* B 112 (2008) 7420; (*d*) X-X. Ke, L. Wang, J-T. Xu, B-Y. Du, Y-F. Tu, Z-Q. Fan, *Soft Matter* 10 (2014) 5201.

[10] (*a*) M. Johnsson, A. Wagenaar, J. B. F. N. Engberts, *J. Am. Chem. Soc.* 125 (2003) 757; (*b*) M. Scarzello, J. E. Klijn, A. Wagenaar, M. C. A. Stuart, R. Hulst, J. B. F. N. Engberts, *Langmuir* 22 (2006) 2558; (*c*) Y. Yang, J. Dong, X. Li, *J. Colloid Interface Sci.* 380 (2012) 83; (*d*) J. Singh, R. Ranganathan, S. Angayarkanny, G. Baskar, A. B. Mandal, *Langmuir* 29 (2013) 5734; (*e*) Z. Jiang, J. Liu, K. Sun, J. Dong, X. Li, S. Mao, Y. Du, M. Liu, *Colloid Polym. Sci.* 292 (2014) 739; (*f*) C. Maiti, R. Banerjee, S. Maiti, D. Dhara, *Langmuir* 31 (2015) 32.

[11] K. Jia, Y. Cheng, X. Liu, X. Li, J. Dong, *RSC Advances* 5 (2015) 640.

[12] W. Li, Y. Yang, T. Luo, J. Zhang, B. Han, *Phys. Chem. Chem. Phys.* 16 (2015) 3640.

[13] (*a*) V. N. Filipovic, M. Bujan, I. Symit, L. Tusek, I. Sytefanic, *J. Colloid Interface Sci.* 201 (1998) 59; (*b*) L. Zhai, M. Zhao, D. Sun, J. Hao, L. Zhang, *J. Phys. Chem.* B 109 (2005) 5627; (*c*) A. Renoncourt, N. Vlachy, P. Bauduin, M. Drechsler, D.Touraud, J-M. Verbavatz, M. Dubois, W. Kunz, B. W. Ninham,

Langmuir 23 (2007) 2376; (*d*) S. H. Tung, H. Y. Lee, S. R. Raghavan, *J. Am. Chem. Soc.* 130 (2008) 8813; (*e*) L. Jiang, K. Wang, M. Deng, Y. Wang, J. Hunag, *Langmuir* 24 (2008) 4600; (*f*) D. Yu, X. Hunag, M. Deng, Y. Lin, L. Jiang, J. Huang, Y. Wang, *J. Phys. Chem.* B 114 (2010) 14955; (*g*) A. Song, S. Dong, X. Jia, J. Hao, W. Liu, T. Liu, *Angew. Chem. Int. Ed.* 117 (2005) 4018; (*h*) X. Li, S. L. Dong, X. F. Jia, A. X. Song, J. C. Hao, *Chem.-Eur. J.* 13 (2007) 9495.

[14] (*a*) C. T. Kresge, M. E. Leonowicz, W. J. Roth, J. C. Vartuli, J. S. Beck, *Nature* 359 (1992) 710; (*b*) M. Rosoff, Vesicles, Marcel Dekker, New York, 1996; (*c*) K. S. Birdi, Surface and Colloid Chemistry, CRC Press, New York, 1997; (*d*) D. F. Evans, H. Wennerstrom, The Colloidal Domain, Where Physics, Chemistry, Biology and Technology Meet, John Wiley, New York, 2nd Ed, 1999; (*e*) A. Makai, E. Csanyi, Z. Nemeth, J. Palinkas, I. Eros, *Int. J. Pharm.* 259 (2003) 95.

[15] C. Wu, Y. Hou, M. Deng, X. Huang, D. Yu, J. Xiang, Y. Liu, Z. Li, Y. Wang, *Langmuir* 26 (2010) 7922.

[16] X. Pei, J. Zhao, X. Wei, *J. Colloid Interface Sci.* 356 (2011) 176.

[17] A. R. Tehrani-Bagha, H. Oskarsson, C. G. van Ginkel, K. Holmberg, *J. Colloid Interface Sci.* 312 (2007) 444.

[18] Y. Fan, Y. Hou, J. Xiang, D. Yu, C. Wu, M. Tian, Y. Han, Y. Wang, *Langmuir* 27 (2011) 10570.

[19] S. Kumar, A. Bhadoria, H. Patel, V. K. Aswal, *J. Phys. Chem.* B 116 (2012) 3699.

[20] M. Villeneuve, R. Ootsu, M. Ishiwata, H. Nakahara, *J. Phys. Chem.* B 110 (2006) 17830.

[21] S. U. Egelhaaf, P. Schurtenberger, *J. Phys. Chem.* 98 (1994) 8560.

[22] R. W. Richards, *Scattering Methods in Polymer Science*, Ellis Horwood Limited, London, 1995.

[23] Y. Yang, L. Liu, X. Huang, X. Tan, T. Luo, W. Li. *Soft Matter* 11 (2015) 8848.

[24] L.M. Zhai, J. Y. Zhang, Q. X. Shi, W. J. Chen and M. Zhao, *J. Colloid Interface Sci.* 284 (2005) 698

[25] R. G. Laughlin, *Colloids Surf.* A 128 (1997) 27.

[26] R. Zana, *Adv. Colloid Interface Sci.* 97 (2002) 205.

[27] P. Somasundaran, Encyclopaedia of Surface and Colloid Science, CRC Press, 2006.

[28] E. Leontidis, *Current Opinion Colloid Interface Sci.* 7 (2002) 81.

[29] A. S. Pandit, M. L. Berkowitz, *Biophys. J.* 82 (2002) 1818.

[30] (*a*) S. Bhattacharya, S. K. Samanata, *J. Phys. Chem. Letter* 2 (2011) 914 (*b*) J. W. Szostak, D. P. Bartel, P. L. Luisi, *Nature* 409 (2001) 387; (*c*) H. H. Zepik, P. Walde, T. Ishikawa, *Angew. Chem. Int. Ed.* 47 (2008) 1323; (*d*) S. S. Mancy, J. P. Schrum, M. Krishnamurthy, S. Tobe, D. A. Treso, J. W. Szostak, *Nature* 454 (2008) 122.